J. Chem. Sci. (2021) 133:43
https://doi.org/10.1007/s12039-021-01904-7

REGULAR ARTICLE

T_2- and T_1 relaxivities and magnetic hyperthermia of iron-oxide nanoparticles combined with paramagnetic Gd complexes

ALEXEY STEPANOV[a,*], SVETLANA FEDORENKO[a], RAFAEL MENDES[b], MARK RÜMMELI[b,c,d,e], LARS GIEBELER[b], BRUNO WEISE[b], THOMAS GEMMING[b], SILVIO DUTZ[f], DIANA ZAHN[f], ILDUS ISMAEV[g], RUSTEM AMIROV[h], KIRILL KHOLIN[a], ALEXANDRA VOLOSHINA[a], ANASTASIYA SAPUNOVA[a], SVETLANA SOLOVIEVA[a] and ASIYA MUSTAFINA[a]

[a]Arbuzov Institute of Organic and Physical Chemistry, FRC Kazan Scientific Center, Russian Academy of Sciences, Arbuzov Str., 8, Kazan, Russia 420088
[b]Leibniz Institute for Solid State and Materials Research Dresden, P.O. Box 270116, 01171 Dresden, Germany
[c]Soochow Institute for Energy and Materials Innovations, College of Energy, Collaborative Innovation Center of Suzhou Nano Science and Technology, Key Laboratory of Advanced Carbon Materials and Wearable Energy Technologies of Jiangsu Province, Soochow University, Suzhou 215006, China
[d]Centre of Polymer and Carbon Materials, Polish Academy of Sciences, M. Curie-Sklodowskiej 34, 41-819 Zabrze, Poland
[e]Institute of Environmental Technology, VŠB-Technical University of Ostrava, 17 Listopadu 15, 708 33 Ostrava, Czech Republic
[f]Institute of Biomedical Engineering and Informatics (BMTI), Technische Universität Ilmenau, Ilmenau, Germany
[g]A.N. Tupolev Kazan Research Technological University, Kazan, Russia 420015
[h]Kazan (Volga Region) Federal University, Kremlyovskaya Str., 18, Kazan, Russia 420008
E-mail: aleksestepanov@yandex.ru

MS received 14 November 2019; accepted 5 March 2021

Abstract. The present paper reports the synthesis of iron-oxide nanoparticles (diameter 12.8±2.2 nm) coated with silica shell doped with paramagnetic Gd(III)-based complexes. The resulting nanoparticles with a silica shell thickness of about 45 nm have an average diameter of 113.1±14.3 nm and feature high transverse and longitudinal relaxivities (356 and 25 mM^{-1} s^{-1}, respectively) at 1.5 T and 25 °C on a medical whole body NMR scanner. It has been also revealed using magnetic heating measurements that the prepared core-shell nanoparticles possess a high specific adsorption rate of around 236 W/g in aqueous media. The surface of the composite nanoparticles was decorated by amino-groups for a greater cellular uptake behaviour. The cell viability measurements reveal the concentration-dependent cytotoxicity of the nanoparticles, which agrees well with the high content of Gd(III) complexes in the nanomaterial. The obtained results show that the core-shell design of nanoparticles with superparamagnetic and paramagnetic parts can be promising for high transverse (and longitudinal) relaxivity as well as magnetic hyperthermia.

Keywords. Gd complexes; Iron-oxide nanoparticles; Magnetic resonance imaging; Hyperthermia.

1. Introduction

In recent decades, iron-oxide nanoparticles and paramagnetic Gd(III) species have gained considerable attention of researches because of their applications in biomedicine where these can be utilized as contrast agents in magnetic resonance imaging (MRI) for visualizing abnormalities in human tissues and organs[1–4] and magnetic hyperthermia (MH) for the elimination of tumour cells.[5–10]

*For correspondence

Supplementary Information: The online version contains supplementary material available at https://doi.org/10.1007/s12039-021-01904-7.

Published online: 22 April 2021

Besides that, iron-oxide nanoparticles have many other applications.[11]

The use of contrast agents is aimed at changing longitudinal (positive contrasting) or transverse (negative contrasting) relaxation times of water protons to gain more contrast between diseased and healthy tissues thereby facilitating forming a diagnosis.[12] Contrast agents may be classified into two main groups. Positive contrast agents reduce longitudinal relaxation time of water protons increasing signal intensity in T_1-weighted images (bright images), whereas negative contrast agents reduce transverse relaxation time of water protons reducing the signal intensity in T_2-weighted images (dark images).[13] Positive contrast agents are usually Gd(III) chelates and some of them such as Magnevist, Dotarem etc have already been approved for clinical use while the negative contrast agents are modified iron-oxide nanoparticles which are also used in clinical examinations (Resovist, Feridex, etc).[14] It must be said that 'single-mode' imaging based on the use of either Gd(III) chelates or iron-oxide nanoparticles suffers from some drawbacks: Gd(III) complexes still have toxicity problems and their blood circulation time is not high enough while the iron-oxide nanoparticles may trigger magnetic susceptibility effects hindering the fault-free imaging which, in turn, complicates accurate diagnostics. In order to reduce these problems, the so-called dual-mode nanoparticulate contrast agents were recently developed and their rational core-shell design was proposed.[15] Such contrast agents combine the superparamagnetic (iron oxides) and paramagnetic materials (Gd(III) species) within one nanoparticle allowing simultaneous obtaining of T_2- or T_1-weighted images removing the need for a re-injection. Besides that, dual-mode contrast agents (CAs) are characterized by enhanced sensitivity, good signal-to-background noise ratio and allow a more precise interpretation of the magnetic resonance images.[15] However, the strong magnetic coupling between superparamagnetic iron-oxides and paramagnetic Gd which quenches T_1 signal when these two materials are located close by[16] is the reason for the specific design of the dual-mode CAs. It is worth noting that silica nanoparticles provide a convenient platform for the embedding of paramagnetic and superparamagnetic building blocks into each nanoparticle.[12,15–18] Moreover, the optimal design of silica nanoparticles doped by paramagnetic complexes [Gd(TCAS)] (shown schematically in Scheme 1) was previously reported.[19] In particular, the impact of the encapsulation mode of [Gd(TCAS)] complexes into silica nanoparticles was clearly demonstrated by tuning the R_1 values from $\sim$ 4.0 mM^{-1} s^{-1} to $\sim$ 50 $mM^{-1}s^{-1}$ (0.47 T, 25 °C).[19]

It is worth noting an extremely useful feature of iron-oxide nanoparticles which is the heat generation when exposed to an alternating magnetic field.[20] The heating of tumour cells using magnetic nanoparticles under alternating magnetic field is called magnetic hyperthermia and may be applied for the killing of tumour cells *in vivo*.[8,20] The heating efficiency of magnetic nanoparticles is characterized by the specific absorption rate (SAR) which is a heat generation ability of a unit mass of biological tissue through the interaction between a magnetic field and magnetic moments of nanoparticles.[8] Many parameters such as size,[10,21] size distribution,[9] aggregation,[9] nanoparticles' shape,[22] phase composition, [20] type of coating,[8,23] amplitude and frequency of the alternating magnetic field,[8,20] concentration[20] have an influence on the heat generation ability of iron-oxide nanoparticles.

Moreover, it is worth noting an efficient cell internalization of the dual-mode CAs as a very important prerequisite of their biomedical application. Convenient surface decoration of silica nanoparticles by amino-groups is the well-known factor facilitating their cell internalization.[24–27]

In view of the aforesaid, herein, we present the silica-coated iron-oxide nanoparticles doped with paramagnetic [Gd(TCAS)] complexes as a primitive concept of novel theranostics capable of dual-mode magnetic resonance imaging and magnetic hyperthermia. Apart from that, the *in vitro* performance of the synthesized nanoparticles on 1.5 T medical whole body NMR scanner as well as cytotoxicity studies towards Chang liver cells is introduced.

2. Experimental

2.1 *Materials*

Commercial chemicals tetraethyl orthosilicate (TEOS) 98%, (3-Aminopropyl)triethoxysilane (APTES) 99%, ammonium hydroxide (28-30%), n-heptanol 98%, cyclohexane 99%, $Gd(NO_3)_3{\cdot}6H_2O$ (99.90%), hexane (97%), acetone (99%), dimethyl sulfoxide (99.9%) were bought from Acros Organics whereas oleic acid (99%), Triton X-100 (98%), NaOH (pellets), octadecane, sodium oleate were obtained from Sigma-Aldrich. Polyvinyl alcohol (Gohsenol-EG-30P) was purchased from Nippon Gohsei. TEOS was purified through vacuum distillation. Ethanol and DMSO were purified using standard procedures whereas all other

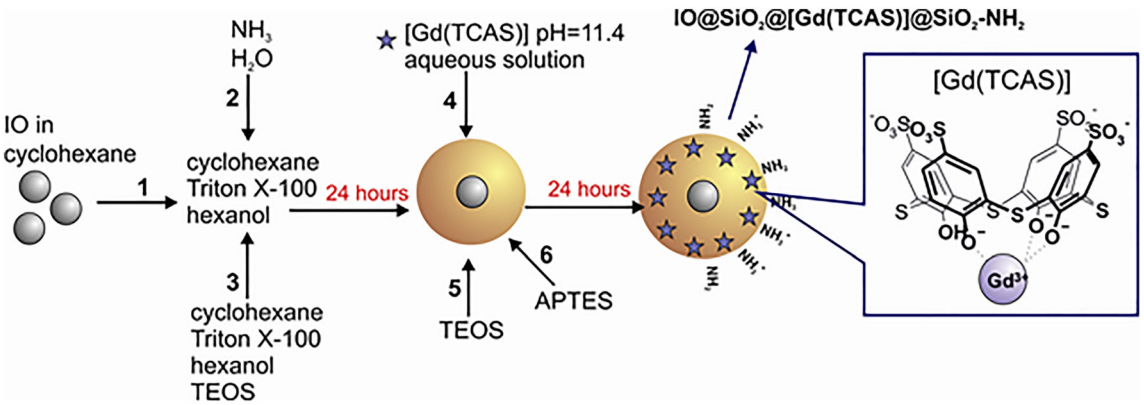

Scheme 1. Schematic representation of synthesis of IO@SiO_2@[Gd(TCAS)]@SiO_2-NH_2 nanoparticles.

chemicals were used as received without further purification.

The standard nutrient medium 'Igla' was bought from the Institute of poliomyelitis and viral encephalitis (Moscow, Russia).

2.1a *Synthesis of p-sulfonatothiacalix[4]arene*: *p*-Sulfonatothiacalix[4]arene (TCAS) has been synthesized according to the well-known literature method.[28]

2.1b *Synthesis of iron oleate*: Iron oleate has been prepared as reported in the literature.[29]

2.1c *Synthesis of 12.8 nm iron-oxide nanoparticles*: The synthesis of 12.8 nm iron-oxide nanoparticles is similar to the synthetic procedure which is reported in our previous paper.[17] However, specifications for the present synthesis is described in the Supplementary data to this article.

2.1d *Synthesis of aminated silica-coated iron-oxide nanoparticles doped with Gd complexes (IO@SiO_2@[Gd(TCAS)]@SiO_2-NH_2)*: The synthe sized oleate-coated iron-oxide nanoparticles (0.02 g) (d ~12.8 nm) were dispersed in 6.15 ml of cyclohexane by ultrasonication in the ultrasound water bath for 60 min. The obtained dispersion was added dropwise by means of a syringe pump with adding the rate of 1 mL/min to the mixture of Triton X-100 (2.98 g), n-heptanol (2.86 mL), and cyclohexane (5.5 mL). After stirring for 10 min, the aqueous solution of NH_3 (0.25 mL of 28-30% NH_3 in 1.38 mL of H_2O) was added, and the mixture was stirred for 30 min. Then, the additionally prepared solution (2.98 g of Triton X-100, 2.86 mL of n-heptanol, 11.65 mL of cyclohexane and 0.25 mL of TEOS) was added to the mixture with the adding rate of 1 mL/min.

After 24 hours of stirring 1.38 mL of an aqueous solution of [Gd(TCAS)] (pH=11.4) was added to the mixture. After 10 min of stirring 0.25 mL of TEOS was added, and in 30 min 0.031 ml of (3-Aminopropyl)triethoxysilane (APTES) were added. Next, following the 24 h stirring at 750 rpm the nanoparticulate phase was separated from the mixture by adding acetone and was then washed with acetone/ethanol mixture (1:1), ethanol by 2X and water by 3X centrifugation/redispersion steps.

2.2 *Physico-chemical characterization*

2.2a *Inductively coupled plasma optical emission spectrometry (ICP-OES)*: Quantitative elemental analysis of the colloids for Fe, Gd and Si was performed using simultaneous inductively coupled plasma optical emission spectrometry (ICP-OES). The details of the experimental parameters for ICP-OES analysis can be found in our previous article.[17]

The experimentally observed Gd (spectral line - 335.047 nm), Fe (spectral line - 259.940 nm) and Si (spectral line - 251.611 nm) concentrations are summarized in Table S1 in the Supplementary Information.

2.2b *HRTEM, TEM and EDX investigations*: The high-resolution transmission electron microscopy (HRTEM) studies of iron-oxide nanoparticles were conducted using FEI Tecnai F30 microscope (operating voltage 300 kV). The samples were prepared from toluene dispersions. The details can be viewed in the Supplementary Information for this paper.

The TEM investigations for IO@SiO_2@[Gd(TCAS)]@SiO_2-NH_2 nanoparticles have been carried out by use of the following procedure. The aqueous dispersion of IO@SiO_2@[Gd(TCAS)]@SiO_2-NH_2 was sonicated using an ultrasound water bath for 5 min and then the volume of about 3 μL was added to 2 mL of acetone. The obtained dispersion was also ultrasonicated for 5 min before dropping onto Lacey Carbon film on a 400 mesh copper TEM grid. The grid was left to dry suspended on the tip of a tweezer on top of a hot plate at 40-50 °C for about 5 min.

The EDX measurements were performed exactly as it was done in reference.[17]

2.2c *FC/ZFC measurements*: The description of FC/ZFC measurements is provided in the Supplementary Information.

2.2d *Dynamic light scattering*: The dynamic light scattering experiment is described in the Supplementary Information to this paper.[17]

2.2e *pH-metry*: Details of pH measurements can be seen in the Supplementary Information for this paper.

2.2f *Relaxometric measurements*: *In vitro* MRI acquisition experiments were performed on a whole-body 1.5 T scanner (ExcelArt Vantage AtlasX, Toshiba, Japan) with a 65-cm horizontal bore size corresponding to a proton resonance frequency of 63,58 MHz. The experimental details for these relaxometric measurements can be viewed in reference[19] in great details.

2.2g *Preparation of the PVA gels containing core-shell silica nanoparticles*: The stable colloids of our core-shell nanoparticles in polyvinyl alcohol (PVA) were prepared as described below. 6.1 mL of hot doubly distilled water (70 °C) were added to 0.2904 g of PVA in a small beaker with a lid. A stiff gel-like structure was formed immediately. Then the gel was vigorously stirred by a magnetic stirrer on a hot plate with hot plate temperature set to 100 °C for 4 h. This was followed by vigorous shaking (~1630 rpm) using vortex set-up for 20 min. Next, the gel was left to stay overnight to get rid of the remaining air bubbles. The next day 0.16 mL of IO@SiO_2@[Gd(TCAS)]@SiO_2-NH_2 dispersion was added to the gel and shook for 30 min (~1630 rpm) on a vortex. The obtained stable dispersion was then transferred into an NMR tube for further *in vitro* MRI investigations.

2.2h *Magnetic hyperthermia measurements*: The specific absorption rate (SAR) was measured by means of magnetic field calorimetry at a field amplitude of up to 25 kA/m and a frequency of 400 kHz, which is a suitable parameter combination for hyperthermia treatment,[30] in a custom-made setup as described before.[31]

For measurement of heating curves, the particle suspensions (0.5 mL in a 2 mL-Eppendorf tube) were placed within the field generating coil. For the temperature measurements, a fibre optic device (Fotemp, OPTOcon, Dresden, Germany) was used and the probe was placed in the centre of the sample. Heating curves were recorded for temperature as a function of time for a duration of one minute. Obtained curves were fitted with suitable mathematical functions (third-degree polynomial) and a temperature drift without magnetic heating (in case of sample temperature is different from the room temperature) was corrected by a linear term. The first derivative of these functions at time point = 0s provides the initial temperature slope (dT/dt) representing the adiabatic case, where all energy is absorbed from a sample and no heat dissipation to the surrounding take place. The SAR was calculated by

$$SAR = \frac{dT}{dt} \cdot \frac{m_s \cdot c}{m_p}$$

where c is the specific heat capacity of the sample, m_s the total mass of the fluid sample and m_p is the mass of the iron oxide particles in the sample. The specific heat capacity of water was used for samples of the here investigates particle concentrations.[10]

2.2i *Cell viability assay*: The effect of the obtained colloids on the cell viability of the cell culture Chang liver from the collection of Institute of Cytology of Russian Academy of Sciences has been determined by fluorescent analysis using system Cytell Cell Imaging (GE Healthcare Life Sciences, Sweden) with Cell Viability BioApp application.[32] The details are described in the Supplementary Information for this paper.

3. Results and Discussion

3.1 *Synthesis and characterization of 12.8 nm iron-oxide nanoparticles*

The oleate-capped iron-oxide nanoparticles have been prepared by thermolysis of iron oleate precursor in the presence of oleic acid as a stabilizer.[29] Then they

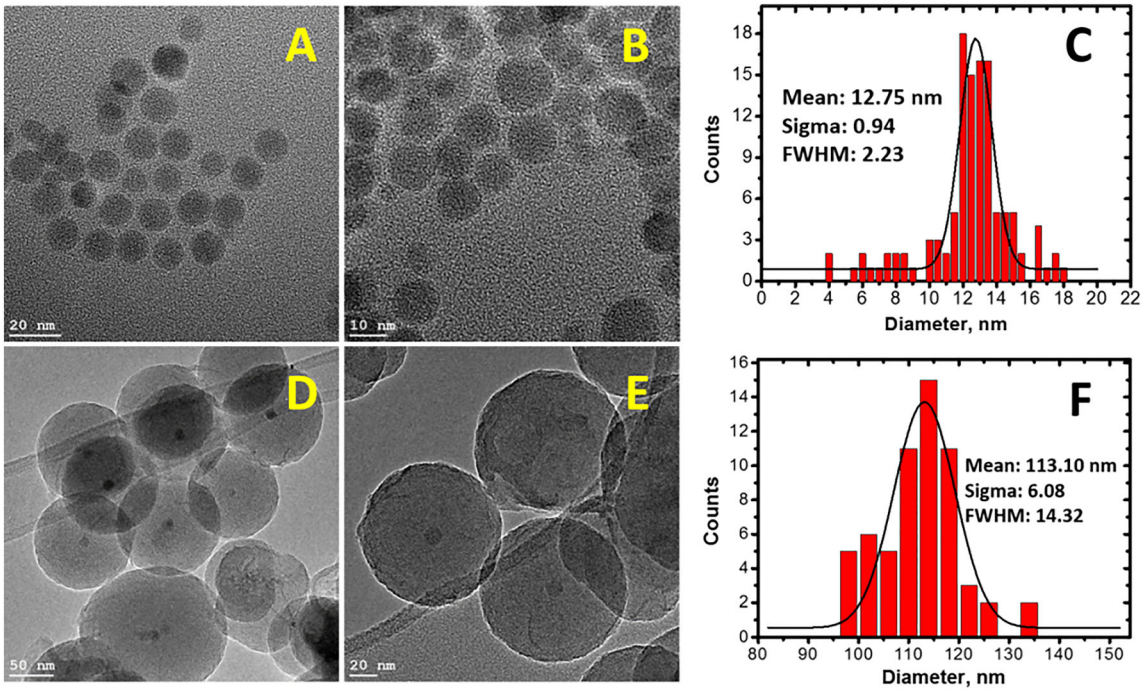

Figure 1. TEM images of oleate-coated iron-oxide nanoparticles (panels A and B), size distribution diagram of iron-oxide nanoparticles (panel C). TEM images of IO@SiO_2@[Gd(TCAS)]@SiO_2-NH_2 nanoparticles (panels D and E), size distribution of IO@SiO_2@[Gd(TCAS)]@SiO_2-NH_2 nanoparticles (panel F).

were imaged by TEM as non-aggregated 12.8±2.2 nm spheres (Figure 1, panel A, B and C). The elemental analysis of the obtained nanoparticles indicates peaks of Cu, Fe, O, C and Si. The Cu peak is conditioned by the copper grid (Figure S1, panel A, Supplementary Information). The peaks of Fe, O, C are related to the elemental composition of oleate-coated iron-oxides, whereas Si peak may come from the glassware (Figure S1, panel A). The XRD analysis of the nanoparticles identifies mixed-phase oxide, namely 84% of Fe_3O_4 (space group *Fd-3m*) and 16% of $Fe_{21.16}O_{31.92}$ (space group $P4_132$) (Figure S1, panel B). The FC/ZFC curves (Figure S1, panel C) of the prepared sample do not coincide due to the reasons specified in our previous paper[33] (Figure 1, panel C). This complicates the precise determination of the blocking temperature of the sample since the derivative of $-(M_{FC} - M_{ZFC})$ with respect to temperature is devoid of clearly-pronounced peaks. The type of magnetism of our iron-oxide nanoparticles was found with M-H measurements which evidenced no hysteresis, coercivity and remnant magnetization (Figure S1, panel D). These experimental findings clearly indicate the superparamagnetism of the synthesized iron oxide nanoparticles at room temperature which is suitable for further biomedical applications.[34]

3.2 *Synthesis of silica nanoparticles bearing superparamagnetic and paramagnetic entities as well as their DLS investigation*

Silica-coated iron-oxide nanoparticles doped with paramagnetic [Gd(TCAS)] complexes have been synthesized by means of the well-known water-in-oil microemulsion procedure.[17–19] The basic concept of this method is the formation of silica as a result of the alkaline hydrolysis of $Si(OC_2H_5)_4$ with subsequent polycondensation of $Si(OH)_4$ into SiO_2. The presence of iron-oxide nanoparticles or water-soluble metal complexes such as [Gd(TCAS)] in the reaction mixture yields the corresponding silica-coated nanoparticles.[17–19] In order to endow the composite nanoparticles with high cellular uptake efficiency and better biocompatibility their surface was modified with primary amino groups by use of (3-Aminopropyl)triethoxysilane in the synthesis (Scheme 1).[35]

TEM investigations of the composite nanoparticles IO@SiO_2@[Gd(TCAS)]@SiO_2-NH_2 confirm the inclusion of iron-oxide cores into silica spheres (Figure 1, panels D and E). The average size of IO@SiO_2@[Gd(TCAS)]@SiO_2-NH_2 nanoparticles was calculated to be about 113.1±14.3 nm whereas silica shell thickness was estimated to be about 45 nm (Figure 1, panels D, E, F).

Also, the TEM analysis also reveals the presence of silica nanoparticles with one, two and several iron-oxide cores as well as silica spheres without magnetic cores (Figure S2 in Supplementary Information), although the latter are to the minor extent over those embedded by the iron oxides. The latter indicates the partial encapsulation of iron-oxides into silica matrix during microemulsion synthesis and, therefore, calls for the quantitative determination of Fe (and Gd) by means of inductively coupled plasma optical emission spectrometry (ICP-OES). The results of this analysis are given in Table S1 (Supplementary Information) and confirm the presence of Fe, Gd, Si in the sample. Based on the ICP-OES data the molar ratio in the nanoparticles was calculated to be about Si:Fe:Gd = 428.3:2.61:1.

Then the obtained aqueous colloids have been studied by means of DLS measurements to reveal their hydrodynamic size, size distribution and charge (Table S2, Supplementary Information).

The IO@SiO_2@[Gd(TCAS)]@SiO_2-NH_2 nanoparticles form aggregates in aqueous suspensions at pH 5.61 and feature size of about 302 nm both by intensity and volume (Table S2) which is consistent with their aggregation evidenced from TEM images. The aggregation of amino-modified nanoparticles is a rather common phenomenon[36–38] resulting from both charge neutralization and interparticle hydrogen bonding due to the presence of amino-ammonium groups at the silica surface. The previously reported excellent colloidal stability of silica-coated iron-oxide nanoparticles without silica surface decoration by amino-groups supports this assumption.[17]

The precise determination of the electrokinetic potential of IO@SiO_2@[Gd(TCAS)]@SiO_2-NH_2 nanoparticles is almost impossible due to their high PDI value (Table S2, Supplementary Information). However, the positive surface charge of IO@SiO_2@[Gd(TCAS)]@SiO_2-NH_2 is rather anticipated at pH 5.61, taking into account the basic nature of the surface primary NH_2 groups. The acidification of the aqueous dispersion of IO@SiO_2@[Gd(TCAS)]@SiO_2-NH_2 to pH of 2.72 did not significantly improve their aggregation behaviour, since the hydrodynamic diameter of IO@SiO_2@[Gd(TCAS)]@SiO_2-NH_2 aggregates reduced from $\sim$ 300 to just $\sim$ 260 nm whereas PDI value remained rather the same (Table S2).

3.3 *Relaxometric and hyperthermia measurements*

Relaxometric efficiency of magnetic probes is determined by their relaxivities which are measured as the slopes of their linear $1/T_{2,1}$ *vs.* C(Fe) or C(Gd) dependencies.[17–19] However, the accurate determination of the magnetic relaxivity values is complicated by the aggregation of the IO@SiO_2@[Gd(TCAS)]@SiO_2-NH_2 colloids.

Therefore, the dispersion of IO@SiO_2@[Gd(TCAS)]@SiO_2-NH_2 in aqueous PVA gel was used to avoid sedimentation of nanoparticles during T_2/T_1 measurements. Relaxometric properties of IO@SiO_2@[Gd(TCAS)]@SiO_2-NH_2 nanoparticles were investigated *in vitro* by means of 1.5T medical NMR scanner. The relaxometric measurements indicate that transverse and longitudinal relaxivities are 356.8±10 $mM^{-1}s^{-1}$ and 25.4±2.0 $mM^{-1}s^{-1}$, respectively (Figure 2). The high R_2/R_1 ratio being about 14 indicates that our core-shell nanoparticles may serve rather as negative contrast agents creating dark images. Consequently, further structure optimization for lowering the R_2/R_1 ratio is necessary for achieving satisfactory dual-mode imaging which is beyond the scope of the present work but will be done in the future.

The heat generation ability of the synthesized nanoparticles has been investigated using magnetic field calorimetry at a field amplitude of 25 kA/m and a frequency of 400 kHz. Taking into consideration the poor solubility of oleate-coated iron-oxide nanoparticles in water their heat generation ability was measured in DMSO dispersions (Figure 3, Panel A).

The SAR value for oleate-capped iron-oxide nanoparticles normalized to the Fe concentration were calculated to be about 127 W/g_{Fe} in DMSO dispersion (362 mM Fe). The SAR value of IO@SiO_2@[Gd(TCAS)]@SiO_2-NH_2 is about 236 W/g_{Fe} in water dispersion (9.78 mM Fe). It is worth noting that the comparison of the heating curves (Figure 3) has no sense since they have different concentrations of Fe, while the SAR values can be compared as they are normalized to the iron content. It is worth noting that both oleate-capped and silica-coated nanoparticles have similar iron-oxide cores. The superparamagnetism of the iron-oxide cores is a prerequisite for the predominant contribution of Néel relaxation into the heating mechanism.[39] Thus, the increased SAR value on going from the oleate- to silica-coated iron-oxide nanoparticles can be explained by the difference in the shell nature and thickness. The literature data introduce the nature of shell or core-shell architecture as a powerful tool to enhance the SAR values[8]. It is worth noting that the silica coating is the factor affecting both rotational movement and aggregation mode of the iron oxide cores. In particular, the size of the silica-coated iron oxides is beyond 100 nm which is the

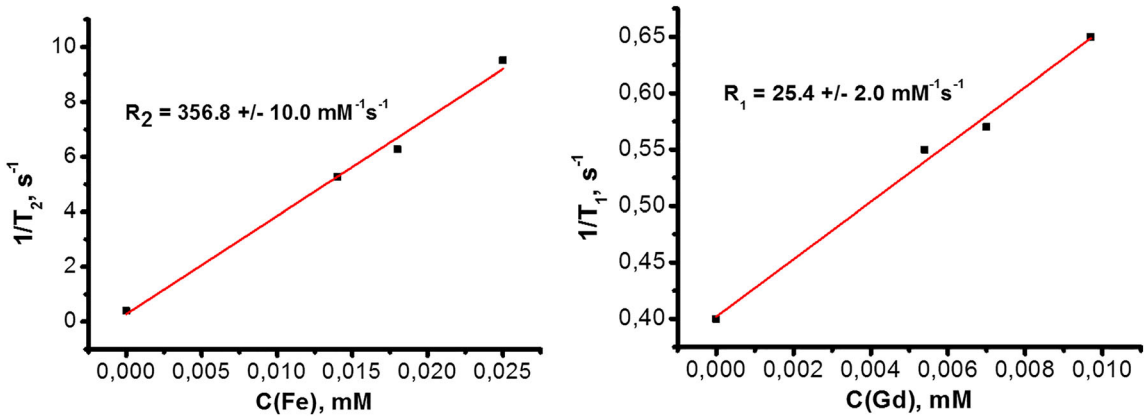

Figure 2. Reciprocal T_2 and T_1 *vs*. Fe and Gd concentrations (1.5 T medical NMR whole-body scanner). PVA mass fraction 4.5%.

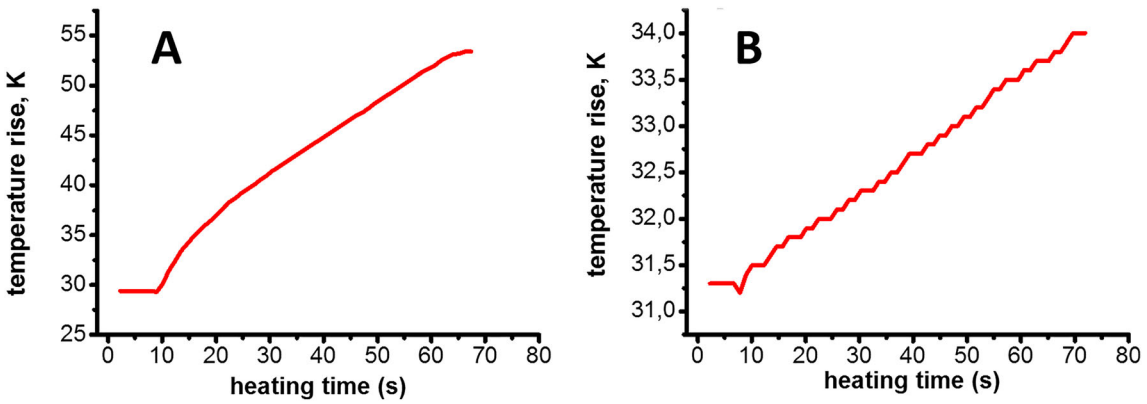

Figure 3. Panel A: heating curve of oleate-coated iron-oxide nanoparticles in DMSO. Panel B: heating curve of IO@SiO_2@[Gd(TCAS)]@SiO_2-NH_2 aqueous dispersion.

reason for a significant decrease in their rotational motion. Moreover, the thick silica shell somewhat restricts the spin interactions of the iron oxide cores versus the oleate-capped iron oxides. Thus, the aggregation of the oleate-capped iron oxides affects their heating capacity in greater extent than the aggregation of IO@SiO_2@[Gd(TCAS)]@SiO_2-NH_2. In order to obtain higher maximal temperature achieved with IO@SiO_2@[Gd(TCAS)]@SiO_2-NH_2 nanoparticles in aqueous dispersions, one should either increase the amplitude and/or frequency of the alternating magnetic field of the hyperthermia set-up or modify the core-shell morphology of the nanoparticles. In particular, the silica shell thickness should be decreased for greater heat generation. However, it is worth noting the great impact of the silica shell thickness on the separation of paramagnetic ([Gd(TCAS)]) and superparamagnetic (IO) components. Thus, the design and synthesis of the nanoparticles with the combination of efficient T_1- and T_2-contrasting capacities with high SAR is a very complicated task that has not been achieved in the present work. Nevertheless, the core-shell design of IO@SiO_2@[Gd(TCAS)]@SiO_2-NH_2 nanoparticles may be a step forward towards creating more sophisticated materials possessing the capability of dual-mode MR imaging and magnetic hyperthermia.

3.4 *Cell viability assay*

The presentation of the cytotoxic effect of IO@SiO_2@[Gd(TCAS)]@SiO_2-NH_2 nanoparticles should be preceded by a discussion of the main mechanisms providing cell death. Poor cell internalization is worth noting as the main reason for the weak cytotoxic effect. However, the surface decoration of silica nanoparticles by amino-groups is the well-known prerequisite for efficient cellular uptake behavior.[35] Literature data reveal the detectable cytotoxic effect of iron oxides, although rather thick silica shell of the iron oxide cores in IO@SiO_2@[Gd(TCAS)]@SiO_2-NH_2 prevents their cytotoxic effect. However, Gd^{3+} ions being encapsulated in the

interfacial layer of IO@SiO_2@[Gd(TCAS)]@SiO_2-NH_2 nanoparticles can be the reason for cytotoxic effect at the high concentrations versus the monomodal silica nanoparticles encapsulated by the iron oxides or [Gd(TCAS)] complexes as the single dopants.[18] The cytotoxicity of the obtained nanoparticles was evaluated by comparison of the cell viability of Chang liver cells after the incubation by various amounts of IO@SiO_2@[Gd(TCAS)]@SiO_2-NH_2 colloids for 24 hours at 37°C as described in the experimental section. Assuming that cytotoxicity originates mainly from Gd(III) ions we have plotted the cell viability against Fe and Ge concentration in the colloids bearing in mind that iron-oxide nanoparticles are known to be less toxic.[40] The cell viability was studied in the range 0.0067-0.055 mM with respect to Gd concentration (corresponding to the range of 0.018–0.141 mM for Fe content) which is outlined in Figure 4 as bar charts.

As follows from Figure 4 Chang liver cells incubated without IO@SiO_2@[Gd(TCAS)]@SiO_2-NH_2 nanoparticles demonstrated 100% viability. The presence of nanoparticles corresponding to 0.018 mM Fe also did not generate any toxic effect on the cells' viability, whereas 0.036 mM Fe decreased the cell viability to about 79% which is still at an acceptable level. The increase of Fe concentration to 0.057 mM lowered the cell viability to approximately 54%, whereas the further rise of Fe (and Gd) content gave rise to zero cell viability (Figure 4, Table S3, Supplementary Information). These data indicate that cytotoxicity of IO@SiO_2@[Gd(TCAS)]@SiO_2-NH_2 nanoparticles towards Chang liver cells is concentration-dependent which is in good agreement with previously obtained results on iron oxide-based nanoparticles.[41,42] It is noteworthy that high cell viability at the concentrations of Fe (0.018 and 0.036 mM) and Gd (0.0067 and 0.014 mM) corresponds to the high transverse and longitudinal relaxation rates of water protons (Figures 2 and 4). This, in turn, is a prerequisite for a good dark and bright contrast, respectively. As follows from Figure 3 (Panel B) 9.78 mM Fe is not enough to raise the temperature to the adequate levels of around 41–45 °C for effective hyperthermia, however, the obtained SAR value of 236 W/g_{Fe} clearly indicates the great potential of the proposed core-shell design for creating of simultaneous dual-mode contrast and magnetic hyperthermia agents.

To sum up, based on the obtained results, further work should be directed towards creating nanoparticles with improved relaxometric and hyperthermic properties. In order to achieve these goals, the following structure optimization must be fulfilled: (1) decreasing the silica layer and increasing the size of the iron-oxide cores for better heating performance, (2) localization of paramagnetic species closer to the interface of nanoparticles in order to rise R_1 value and to lower R_2/R_1 ratio for satisfactory simultaneous bright and dark contrast, (3) better adaptation of field parameters to the magnetic properties of the particles during hyperthermia experiments, (4) improvement of colloidal stability of nanoparticles in aqueous dispersions. Besides that, the compatibility of the developed nanoparticles with blood must be tested which is beyond the scope of the present paper and will be done in the nearest future.

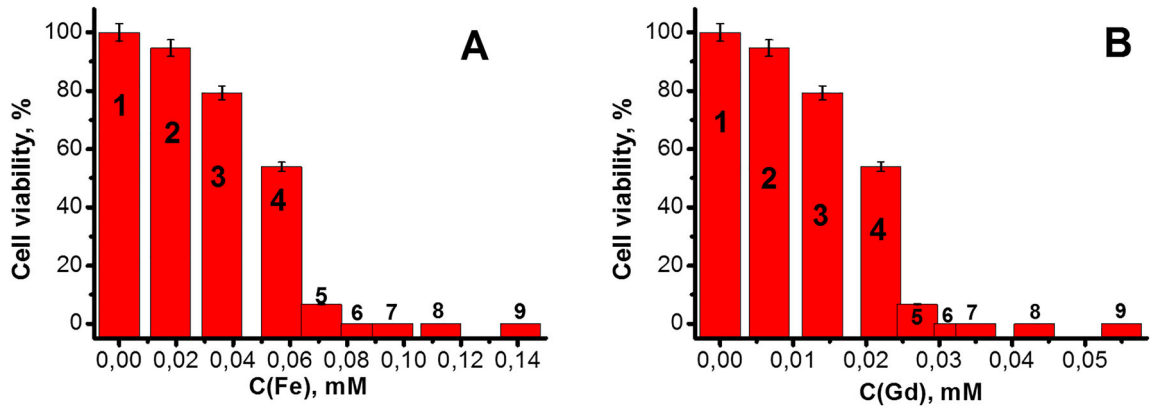

Figure 4. Panel A: cell viability of Chang liver cells incubated without (1) and with IO@SiO_2@[Gd(TCAS)]@SiO_2-NH_2 nanoparticles: (2) 0.018 mM Fe, (3) 0.036 mM Fe, (4) 0.057 mM Fe, (5) 0.071 mM Fe, (6) 0.085 mM Fe, (7) 0.096 mM Fe, (8) 0.113 mM Fe, (9) 0.141 mM Fe. Panel B: cell viability of Chang liver cells incubated without (1) and with IO@SiO_2@[Gd(TCAS)]@SiO_2-NH_2 nanoparticles: (2) 0.0067 mM Gd, (3) 0.014 mM Gd, (4) 0.022 mM Gd, (5) 0.027 mM Gd, (6) 0.032 mM Gd, (7) 0.035 mM Gd, (8) 0.043 mM Gd, (9) 0.054 mM Gd. Error bars signify standard deviations of the cell viability assay determined from three measurements.

4. Conclusions

On the whole, we have synthesized nanoparticles combining superparamagnetic and paramagnetic components in a single probe using a core-shell design. The paramagnetic component residing in the silica matrix ([Gd(TCAS)]) is responsible for longitudinal relaxivity, whereas the superparamagnetic component (iron-oxide) accounts for both the high transverse relaxivity and magnetic heating ability of our nanoparticles. High values of transverse and longitudinal relaxivities along with more or less good heat generation ability of the obtained core-shell nanoparticles as well as negligible cytotoxicity at certain concentrations makes the proposed nanoparticulate core-shell design promising for further improvement and testing as dual-mode contrast agents for magnetic resonance imaging (MRI), while their efficiency as hyperthermia agents for tumour elimination requires a longer hyperthermia treatment duration and greater amplitude and/or frequency of the alternating magnetic field. The surface decoration by amino-groups is aimed at enhancing the cell internalization of the composite nanoparticles. The cell viability measurements revealed the concentrations of the composite nanoparticles which are enough for both significant T_1- and T_2-contrasting effects quantitatively revealed by the whole-body scanner and the low cytotoxic effect. To the best of our knowledge, the present work is among the rare examples of high relaxivities along with heat generation ability.

Supplementary Information (SI)

The supplementary information (SI) to this paper contains a description of the following measurements: FC/ZFC, XRD, HRTEM, dynamic light scattering (DLS), pH-metry and relaxometric measurements. The SI also has the EDX and XRD patterns, the elemental composition of core-shell nanoparticles IO@SiO_2@[Gd(TCAS)], DLS data for the aqueous IO@SiO_2@[Gd(TCAS)]@SiO_2-NH_2 colloids, cell viability of Chang liver cells at different nanoparticles' concentration, TEM images of IO@SiO_2@[Gd(TCAS)]@SiO_2-NH_2 nanoparticles. Supplementary information is available at www.ias.ac.in/chemsci.

Acknowledgement

The work was funded by the Government assignment for FRC Kazan Scientific Center of Russian academy of Science (Reg. Nr. AAAA-A18-118041760011-2). M.R. thanks National Science Foundation of China (Grant No. 52071225) and the Czech Republic under the ERDF program "Institute of Environmental Technology—Excellent Research" (No. CZ.02.1.01/0.0/0.0/16_019/0000853).

References

1. Jedlovszky-Hajdu A, Tombacz E, Banyai I, Babos M and Palko A 2012 Carboxylated magnetic nanoparticles as MRI contrast agents: Relaxation measurements at different field strengths *J. Magn. Magn. Mater.* **324** 3173
2. Xiao N, Gu W, Wang H, Deng Y, Shi X and Ye L 2014 T_1–T_2 dual-modal MRI of brain gliomas using PEGylated Gd-doped iron oxide nanoparticles *J. Colloid Interface Sci.* **417** 159
3. Sulek S, Mammadov B, Mahcicek D I, Sozeri H, Atalar E, Tekinay A B and Guler M O 2011 Peptide functionalized superparamagnetic nanoparticles as MRI contrast agents *J. Mater. Chem.* **21** 15157
4. Huang J, Wang L, Lin R, Wang A Y, Yang L, Kuang M, et al. 2013 Casein-coated iron oxide nanoparticles for high MRI contrast enhancement and efficient cell targeting *ACS App. Mater. Interfaces.* **5** 4632
5. Ansari L and Malaekeh-Nikouei B 2017 Magnetic silica nanocomposites for hyperthermia applications *Int. J. Hyperth.* **33** 354
6. Laurent S, Dutz S, Häfeli U O and Mahmoudi M 2011 Magnetic fluid hyperthermia: focus on superparamagnetic iron-oxide nanoparticles *Adv. Colloid Interface Sci.* **166** 8
7. Gonzales-Weimuller M, Zeisberger M and Krishnan K M 2009 Size-dependent heating rates of iron oxide nanoparticles for magnetic fluid hyperthermia *J. Magn. Magn. Mater.* **321** 1947
8. Hedayatnasab Z, Abnisa F and Duad W M A W 2017 Review on magnetic nanoparticles for magnetic nanofluid hyperthermia applications *Mater. Des.* **123** 174
9. Guibert C, Dupuis V, Peyre V and Fresnais J 2015 Hyperthermia of magnetic nanoparticles: experimental study of the role of aggregation *J. Phys. Chem. C* **119** 28148
10. Müller R, Dutz S, Neeb A, Cato A C B and Zeisberger M 2013 Magnetic heating effect of nanoparticles with different sizes and size distributions *J. Magn. Magn. Mater.* **328** 80
11. Ramimoghadam D, Bagheri S and Hamid S B A 2014 Progress in electrochemical synthesis of magnetite iron oxide nanoparticles *J. Magn. Magn. Mater.* **368** 207
12. Yang M, Gao L, Liu K, Luo C, Wang Y, Yu L and Peng H 2015 Characterization of Fe_3O_4/SiO_2/$Gd_2O(CO_3)_2$ core/shell/shell nanoparticles as T1 and T2 dual mode MRI contrast agent *Talanta* **131** 661
13. Xiao W, Gu H, Li D, Chen D, Deng X, Jiao Z and Lin J 2012 Microwave-assisted synthesis of magnetite nanoparticles for MRI blood pool contrast agents *J. Magn. Magn. Mater.* **324** 488
14. Rohrer M, Bauer H, Mintorovitch J, Requardt M and Weinmann H J 2005 Comparison of magnetic properties of MRI contrast media solutions at different magnetic field strengths *Invest. Radiol.* **40** 715
15. Shin T-H, Choi J S, Yun S, Kim I S, Song H T, Kim Y, et al. 2014 T1 and T2 dual-mode MRI contrast agent for enhancing accuracy by engineered nanomaterials *ACS Nano* **8** 3393

16. Choi J-S, Lee J H, Shin T H, Song H T, Kim E Y and Cheon J 2010 Self-confirming "AND" logic nanoparticles for fault-free MRI *J. Am. Chem. Soc.* **132** 11015
17. Stepanov A, Fedorenko S, Amirov R, Nizameev I, Kholin K, Voloshina A, et al. 2018 Silica-coated iron-oxide nanoparticles doped with Gd(III) complexes as potential double contrast agents for magnetic resonance imaging at different field strengths *J. Chem. Sci.* **130** 125
18. Fedorenko S, Stepanov A, Zairov R, Kaman O, Amirov R, Nizameev I, Kholin K, Ismaev I, Voloshina A, Sapunova A, Kadirov M and Mustafina A 2018 One-pot embedding of iron oxides and Gd(III) complexes into silica nanoparticles—Morphology and aggregation effects on MRI dual contrasting ability *Colloids Surf., A* **559** 60
19. Fedorenko S V, Grechkina S L, Mustafina A R, Kholin K V, Stepanov A S, Nizameev I R, Ismaev I E, Kadirov M K, Zairov R R, Fattakhova A N, Amirov R R and Soloveva S E 2017 Tuning the non-covalent confinement of Gd(III) complexes in silica nanoparticles for high T1-weighted MR imaging capability *Colloids Surf., B* **149** 243
20. Abenojar E C, Wickramasinghe S, Bas-Concepcion J and Samia A C S 2016 Structural effects on the magnetic hyperthermia properties of iron oxide nanoparticles *Prog. Nat. Sci.* **26** 440
21. Parmar H, Smolkova IS, Kazantseva N E, Babayan V, Smolka P, Moucka R, et al. 2015 Size dependent heating efficiency of iron-oxide single domain nanoparticles *Proced. Eng.* **102** 527
22. Nemati Z, Das R, Alonso J, Clements E, Phan M H and Srikanth H 2017 Iron oxide nanospheres and nanocubes for magnetic hyperthermia therapy: a comparative study *J. Electron. Mater.* **46** 3764
23. Xiao L L, Fan H M, Yi J B, Yang Y, Choo E S G, Xue J M, et al. 2012 Optimization of surface coating on Fe_3O_4 nanoparticles for high performance magnetic hyperthermia agents *J. Mater. Chem.* **22** 8235
24. Fedorenko S V, Mustafina A R, Mukhametshina A R, Jilkin M E,. Mukhametzyanov T A, Solovieva A O, Pozmogova T N, Shestopalova L V, Shestopalov M A, Kholin K V, Osin Y N and Sinyashin O G 2017 Cellular imaging by green luminescence of Tb(III)-doped aminomodified silica nanoparticles *Mater. Sci. Eng., C* **76** 551
25. Beddoes C M, Case C P and Briscoe W H 2015 Understanding nanoparticle cellular entry: a physicochemical perspective *Adv. Colloid Interface Sci.* **218** 48
26. Salatin S, Dizaj S M and Khosroushahi A Y 2015 Effect of the surface modification, size, and shape on cellular uptake of nanoparticles *Cell Biol. Int.* **39** 881
27. Saha K, Kim S T, Yan B, Miranda O R, Alfonso F S, Shlosman D and Rotello V M 2013 Surface functionality of nanoparticles determines cellular uptake mechanisms in mammalian cells *Small* **9** 300
28. Iki N, Fujimoto T and Miyano S 1998 A new water-soluble host molecule derived from thiacalixarene *Chem. Lett.* **27** 625
29. Bronstein L M, Huang X, Retrum J, Schmucker A, Pink M, Stein B D and Dragnea B 2007 Influence of iron oleate complex on iron oxide nanoparticle formation *Chem. Mater.* **19** 3624
30. Dutz S, Kettering M, Hilger I, Müller R and Zeisberger M 2011 Magnetic multicore nanoparticles for hyperthermia—influence of particle immobilization in tumour tissue on magnetic properties *Nanotechnology* **22** 265102
31. Dutz S, Müller R, Eberbeck D, Hilger I and Zeisberger M 2015 Magnetic nanoparticles adapted for specific biomedical applications *Biomed. Eng.-Biomed. Tech.* **60** 405
32. Voloshina D, Semenov V E, Strobykina A S, Kulik N V, Krylova E S, Zobov V V and Reznik V S 2017 Synthesis and antimicrobial and toxic properties of novel 1,3-bis(alkyl)-6-methyluracil derivatives containing 1,2,3- and 1,2,4-triazolium fragments *Russ. J. Bioorg. Chem.* **43** 170
33. Fedorenko S, Stepanov A, Sibgatullina G, Samigullin D, Mukhitov A, Petrov K, et al. 2019 Fluorescent magnetic nanoparticles for modulating the level of Ca^{2+} in motoneurons *Nanoscale* **11** 16103
34. Iqbal Y, Bae H, Rhee I and Hong S 2016 Magnetic heating of silica-coated manganese ferrite nanoparticles *J. Magn. Magn. Mater.* **409** 80
35. Zhu X M, Wang Y X, Leung K C, Lee S F, Zhao F, Wang D W, et al. 2012 Enhanced cellular uptake of aminosilane-coated superparamagnetic iron oxide nanoparticles in mammalian cell lines *Int. J. Nanomed.* **7** 953
36. Fedorenko S V, Mustafina A R, Mukhametshina A R, Jilkin M E, Mukhametzyanov T A, Solovieva A O, et al. 2017 Cellular imaging by green luminescence of Tb(III)-doped aminomodified silica nanoparticles *Mater. Sci. Eng. C* **76** 551
37. Davydov N, Mustafina A, Burilov V, Zvereva E, Katsyuba S, Vagapova L, et al. 2012 Complex formation of d-metal ions at the interface of TbIII-doped silica nanoparticles as a basis of substrate-responsive TbIII-centered luminescence *ChemPhysChem.* **13** 3357
38. Mukhametshina A R, Fedorenko S V, Petrov A M, Zakyrjanova G F, Petrov K A, Nurullin L F, et al. 2018 Targeted nanoparticles for selective marking of neuromuscular junctions and ex vivo monitoring of endogenous acetylcholine hydrolysis *ACS Appl. Mater. Interfaces* **10** 14948
39. Rosensweig R E 2002 Heating magnetic fluid with alternating magnetic field *J. Magn. Magn. Mater.* **252** 370
40. Lübbe A S, Alexiou C and Bergemann C 2001 Clinical applications of magnetic drug targeting *J. Surg. Res.* **95** 200
41. Mendes R G, Koch B, Bachmatiuk A, El-Gendy A A, Krupskaya Y, Springer A, et al. 2014 Synthesis and toxicity characterization of carbon coated iron oxide nanoparticles with highly defined size distributions *Biochim. Biophys. Acta* **1840** 160
42. Haddad P S, Santos M C, Guzzi Cassago C A, Bernardes JS , Jesus M D and Seabra A B 2016 Synthesis, characterization, and cytotoxicity of glutathione-PEG-iron oxide magnetic nanoparticles *J. Nanopart Res.* **18** 369